Check for
updates

On the Relation Between Transition Region Network Jets and Coronal Plumes

Youqian Qi[1] · Zhenghua Huang[1] · Lidong Xia[1] 🔾 **·
Bo Li[1] · Hui Fu[1] · Weixin Liu[1] · Mingzhe Sun[1] ·
Zhenyong Hou[1]**

Abstract Both coronal plumes and network jets are rooted in network lanes. The relationship between the two, however, has yet to be addressed. For this purpose, we perform an observational analysis using images acquired on 2015 December 4 with the *Atmospheric Imaging Assembly* (AIA) 171 Å passband to follow the evolution of coronal plumes, the observations taken by the *Interface Region Imaging Spectrograph* (IRIS) at slit-jaw 1330 Å to study the network jets, and the line-of-sight magnetograms taken by the *Helioseismic and Magnetic Imager* (HMI) to overview the photospheric magnetic features in the regions. Four regions in the network lanes are identified and labeled R1–R4, which are abundant with network jets. R1 and R2 are associated with coronal plumes that could be clearly seen for at least five days, while coronal plumes are hardly seen in R3 and R4 for at least three days. Furthermore, while magnetic features in all these regions are dominated by positive polarity, they are more compact (suggesting stronger convergence) in R1 and R2 than that in R3 and R4. We develop an automated method to identify and track the network jets in the regions. We find that the network jets rooted in R1 and R2 are higher and faster than those in R3 and R4, indicating that network regions producing stronger coronal plumes also tend to produce more dynamic network jets. We suggest that the stronger convergence in R1 and R2 might provide a condition for faster shocks and/or more small-scale magnetic reconnection events that power more dynamic network jets and coronal plumes.

✉ L. Xia
  xld@sdu.edu.cn

  Y. Qi
  qiyq@mail.sdu.edu.cn

[1] Shandong Provincial Key Laboratory of Optical Astronomy and Solar-Terrestrial Environment,
   Institute of Space Sciences, Shandong University, Weihai, 264209 Shandong, China

1. Introduction

Coronal plumes (or rays) are bright ray-like features in the corona that could extend to tens of solar radii (see *e.g.* Deforest *et al.*, 1997; DeForest, Plunkett, and Andrews, 2001). They were first found in polar coronal holes during the eclipse more than 100 years ago (see descriptions of the observations in van de Hulst, 1950). Coronal plumes have also been identified in UV, EUV and X-ray, such observations having become available in the space era. With *Skylab* observations at Mg IX, Wang and Sheeley (1995) first identified plume-like features in the low-latitude coronal holes, and they proposed that coronal plumes are not unique in the polar region but may occur in an open field region at any latitudes on the Sun. This has been confirmed by observations from SOHO, TRACE, *Hinode*, STEREO and SDO (*e.g.* Del Zanna and Bromage, 1999; Del Zanna, Bromage, and Mason, 2003; Wang and Muglach, 2008; Feng *et al.*, 2009; Tian *et al.*, 2011a; Yang *et al.*, 2011; DeForest *et al.*, 2018). The electron density of coronal plumes is 3 – 8 times larger than that in the inter-plume region (see Wilhelm *et al.*, 2011, and the references therein), and their lifetimes range from ∼ 20 hours (Lamy *et al.*, 1997) to days (Withbroe, Feldman, and Ahluwalia, 1991; Young, Klimchuk, and Mason, 1999; DeForest, Lamy, and Llebaria, 2001). Since coronal plumes are always present in coronal holes which are the major source of fast solar wind (*e.g.* Xia, Marsch, and Curdt, 2003; Xia, Marsch, and Wilhelm, 2004; Cranmer, 2009; Madjarska *et al.*, 2012; Fu *et al.*, 2015), the connection between coronal plumes and the solar wind has been studied intensively. Some have indicated that they might feed sufficient plasma and energy into the fast solar wind (see *e.g.* Velli, Habbal, and Esser, 1994; Gabriel, Bely-Dubau, and Lemaire, 2003; Gabriel *et al.*, 2005; Tian *et al.*, 2010, 2011a; Fu *et al.*, 2014; Liu *et al.*, 2015), although they might be not the major source (see *e.g.* Wang, 1994; Habbal *et al.*, 1995; Hassler *et al.*, 1999; Patsourakos and Vial, 2000; Giordano *et al.*, 2000; Wilhelm *et al.*, 2000; Teriaca *et al.*, 2003). More details about the history of the observations of coronal plumes could be found in recent reviews (Wilhelm *et al.*, 2011; Poletto, 2015).

Coronal plumes are classified into two types, beam plumes and network plumes (Gabriel *et al.*, 2009). Beam plumes have (quasi-)cylindrical shape with a base diameter of 20 – 30 Mm at about 30 Mm off the surface of the Sun (see *e.g.* Deforest *et al.*, 1997), and their footpoints normally correspond to coronal bright points (*e.g.* Wang, 1998; Wang and Muglach, 2008; Pucci *et al.*, 2014). Network plumes (also named "curtain plumes") are made up of many faint structures that are aligned in a curtain shape (Gabriel, Bely-Dubau, and Lemaire, 2003). Network plumes are rooted in regions along the edge of supergranular boundaries that correspond to network lanes in the chromosphere (Gabriel *et al.*, 2009; Rincon and Rieutord, 2018).

Both types of coronal plumes are associated with bright network lanes, where the associated magnetic features are dominated by unipolarity (see *e.g.* Newkirk and Harvey, 1968; Wang and Sheeley, 1995; Wang *et al.*, 1997; Deforest *et al.*, 1997; Wang and Muglach, 2008; Wang, Warren, and Muglach, 2016; Avallone *et al.*, 2018). Recently, by investigating the evolution of the magnetic features associated with tens of coronal plumes as observed by HMI, Wang, Warren, and Muglach (2016) found that coronal plumes form where unipolar network elements inside coronal holes converge to form dense clumps and fade as the clumps disperse again. Similar results have been confirmed by Avallone *et al.* (2018), who also made a quantitative analysis and found that coronal plumes appear when convergence of

the associated magnetic flux surpasses a flux density of $\sim 200-600$ Mx cm^{-2}. Along with the dominant polarity, small bipolar features also frequently appear nearby and might be canceling with the dominant unipolarity (*e.g.* Wang and Sheeley, 1995; Wang *et al.*, 1997; Wang and Muglach, 2008). Based on the behaviors of magnetic features in the footpoints of the coronal plumes, Wang and Sheeley (1995) proposed a magnetic reconnection scenario, in which reconnection occurs between open fields (corresponding to the dominant unipolarity) and nearby small-scale loops (corresponding to the small bipolar features). Energy dissipation due to such magnetic reconnection process should take place at the base of the corona (Wang, 1994). The released energy in the magnetic reconnection might conduct downward to the chromosphere and result in plasma evaporation, which maintains the high density in the coronal plumes (Wang, 1998).

Many studies have focused on the connection between coronal plumes and other dynamic phenomena in the solar atmosphere. For coronal plumes with coronal bright points persisting at their bases, studies found that they appear several hours after the coronal bright points first appeared and fade away hours after the coronal bright points disappeared (Wang, 1998; Wang and Muglach, 2008; Pucci *et al.*, 2014). While coronal jets are also closely linked to bipolar regions with one dominant polarity (see *e.g.* Doschek *et al.*, 2010; Huang *et al.*, 2012; Sterling *et al.*, 2015; Panesar *et al.*, 2016; Panesar, Sterling, and Moore, 2018; Panesar *et al.*, 2018), the connection between coronal jets and coronal plumes has also been investigated. Using white light observations during the eclipse data and EIT 195 Å data from SOHO, Lites *et al.* (1999) reported that a polar coronal plume was disturbed by a jet with a speed of ~ 200 km s^{-1} embedded therein. Raouafi *et al.* (2008) showed that over 90% of the 28 studied jets were associated with plumes, and they also found that 70% of those plume-related jets were followed by plume haze occurring minutes to hours later while the rest of the jets resulted in brightness enhancement in the pre-existed plumes. In more recent studies, the close relationship between coronal plumes and coronal jets has been confirmed (Raouafi and Stenborg, 2014; Panesar *et al.*, 2018). They further found that a large number of small jets and transient bright points frequently occurring in the bases of coronal plumes could be the main energy source for coronal plumes. A more comprehensive summary on the relation between jets and coronal plumes could be found in a state-of-the-art review article by Raouafi *et al.* (2016).

Recently, using the high resolution observations of the transition region from the *Interface Region Imaging Spectrograph* (IRIS), Tian *et al.* (2014) discovered that networks in the upper chromosphere and transition region of coronal holes are occupied by numerous small-scale jets (hereafter, network jets). Network jets having lifetimes of $20-80$ s and speeds of $80-250$ km s^{-1} are prevalent in the network regions. They have been suggested to be powered by magnetic reconnection and many of them were found to be heated to at least 10^5 K. Network jets have also been found in quiet-sun regions to be slower and shorter than those in coronal holes (Narang *et al.*, 2016; Kayshap *et al.*, 2018).

Since both coronal plumes and network jets are rooted in the network and both of them might be powered by magnetic reconnection, one would naturally ask the question: what is the relationship between the two phenomena? To investigate this point, we analyze a set of IRIS and SDO coordinated observations of network regions to see whether or not there are evident differences in the dynamics of coronal plumes and network jets. We develop an automatic method to identify and track jets in the network regions. With this method, we obtain birth rates, lifetimes, lengths and speeds of the network jets. We then compare these parameters obtained for different parts of the network regions.

The paper is organized as follows: the observations and the data analysis techniques are described in Section 2 (see also the Appendix for the description of the algorithm); the

results of the analysis are shown in Sections 3 and 4; the discussion is given in Section 5 and the conclusions are presented in Section 6.

2. Observations and Data Analysis

2.1. Details of Observations

The data were taken on 2015 December 4 from 01:21 UT to 02:19 UT. They were collected by IRIS (De Pontieu *et al.*, 2014) and the *Atmospheric Imaging Assembly* (AIA, Lemen *et al.*, 2012) and the *Helioseismic and Magnetic Imager* (HMI, Schou *et al.*, 2012) aboard the *Solar Dynamics Observatory* (SDO, Pesnell, Thompson, and Chamberlin, 2012).

IRIS was operated in a very large sit-and-stare mode and the IRIS slit-jaw (SJ) imager was observing only at 1330 Å passband with a cadence of 9 s. The spatial scale of the IRIS SJ images is $0.167'' \times 0.167''$. In order to reduce the telemetry load, the data had been binned by 2×2 pixels and thus the spatial scale of each grid of the data array is $0.334'' \times 0.334''$. The level 2 IRIS data are used and no further calibration is required.

The AIA and HMI data were downloaded from JSOC. The analyzed AIA data are taken in 1600 Å and 171 Å passbands. The cadences of the AIA 1600 Å and 171 Å data are 24 s and 12 s, respectively. The pixel size of the AIA data is $0.6'' \times 0.6''$. The HMI line-of-sight magnetograms with a cadence of 45 s and a pixel size of $0.6'' \times 0.6''$ are used. The AIA and HMI data are prepared with standard procedures provided by the instrument teams, and the level 1.5 data are analyzed.

The images taken from different passbands are aligned using as reference several features (such as obvious bright points/dots) in the images. We first align IRIS 1330 Å images to AIA 1600 Å, and then HMI magnetograms to AIA 1600 Å. Although images from different passbands of AIA have been aligned with each other by the data processing pipeline, we also checked the alignment between 1600 Å and 171 Å using referent features and found an offset of $1''$ at both Solar_X and Solar_Y directions.

In Figure 1, we show the context of the region-of-interest taken with AIA, HMI and IRIS around 01:21 UT. The region includes the boundary of an on-disk coronal hole (see Figure 1(a)). We can see that the region consists of a cluster of positive magnetic features (Figure 1(b)), which are aligned in a typical magnetic structure of network regions (see *e.g.* Xia, Marsch, and Curdt, 2003; Xia, Marsch, and Wilhelm, 2004). The dominant polarities are in line with the coronal hole seen in the AIA data. The network regions could be clearly seen in AIA 1600 Å and IRIS SJ 1330 Å images (see the bright lanes in Figures 1(c) and (d)). Many jets rooted in the network lanes are found, and they can be clearly seen in the IRIS SJ 1330 Å images. In AIA 171 Å images (Figures 1(a) and (e)), we can see that a set of plume-like features are rooted in some of the regions.

2.2. Network Jet Identification and Tracking

Because network jets are extremely abundant in network regions, in order to identify and track them, we have developed an automatic method that is briefly described in this section. If a feature is brighter than 2.5 times of the background and extended for more than $4''$ from the base near a network lane, it is considered as a jet-like feature. An identified jet-like feature is then traced back and forth in time to obtain its evolution. The height of a jet-like feature is determined by the distance between the base and the point along its propagation direction where its brightness drops below 2.5 times of that of the background. If a jet-like
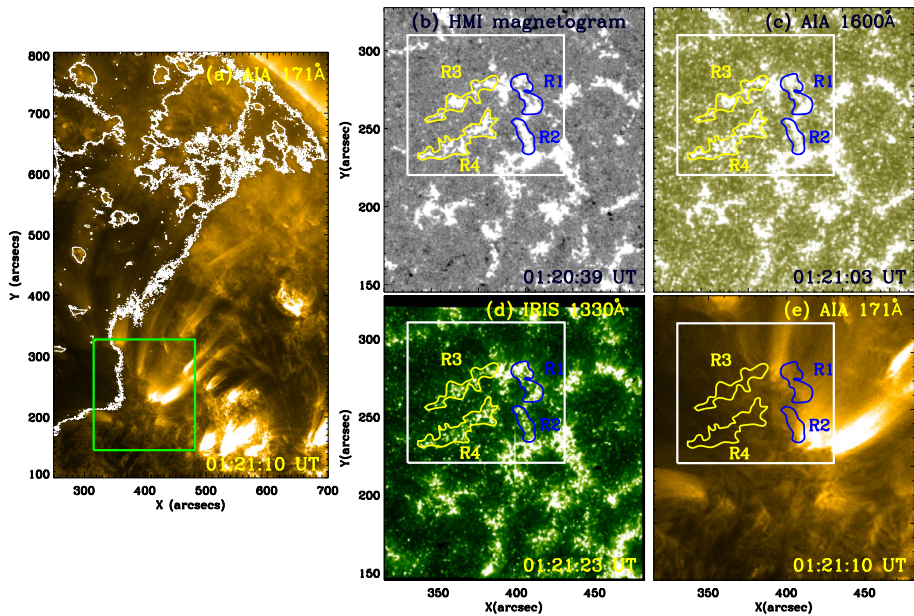
Figure 1 Context images for regions studied in the present work taken on 2015 December 4. (**a**) The AIA 171 Å image giving an overview of the coronal structures in and around the studied regions. The contours (*white lines*) outline the boundaries of the coronal hole determined in the AIA 193 Å image. The region enclosed by the rectangle (*green lines*) is zoomed-in in panels (**b**–**e**), where shown are HMI magnetic features (**b**), AIA 1600 Å image (**c**), IRIS SJ 1330 Å image (**d**), and AIA 171 Å image (**e**). The rectangles (*white lines*) in panels (**b**)–(**e**) give the field-of-view used for jet identification and tracking. The regions outlined by *blue lines* with the markings of R1 and R2 are the network regions where coronal plumes are clearly present. The regions outlined by *yellow lines* with the markings of R3 and R4 are the network regions where coronal plumes are hardly seen.

feature can be recognized in more than one frame and its height is changing with time, it is considered as a network jet. By determining the heights of a jet changing with time, its speed can be obtained. More details of the algorithm can be found in the Appendix.

3. Dynamics in the Network Regions

The region observed by IRIS SJ 1330 Å and by AIA at 171 Å that has been analyzed in this paper is shown in Figure 1 and the time evolution of the features is shown in the associated online animation. In the IRIS SJ 1330 Å images, we can see that jets are abundant in the network lanes. The network jets are fine and dynamic, which are the typical characteristics of these phenomena (Tian *et al.*, 2014). In regions R1–R4, the network jets ejected in directions almost parallel to each other, which allows our automatic algorithm to be used (see the Appendix for details). In AIA 171 Å images, it is clear that plume-like features are rooted in the regions of R1 and R2, while they are hardly seen (or too weak to be seen) in the regions of R3 and R4. The selection of these regions is based on the fact that their connections (if any) to the coronal plumes could be confirmed with no doubt for a few days. By tracing these regions in AIA observations, the coronal plumes rooted in R1 and R2 could be clearly seen from December 1 to 6 and there was no clear coronal plume
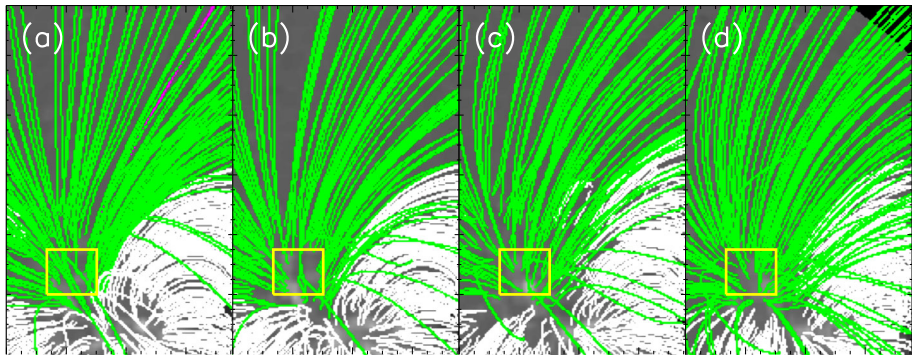
Figure 2 The magnetic field lines in the regions derived from the potential field extrapolations based on HMI data taken on December 1 (**a**), December 2 (**b**), December 3 (**c**) and December 4 (**d**). The *green and purple lines* are representative of open field lines and the *white ones* are closed field lines. The *yellow rectangles* indicate the studied region as shown in Figure 1(b) – (e).

associated with R3 and R4 from December 3 to 6. Meanwhile, the other network regions are located in more complex regions such as regions too close to active region loops or in the back of coronal plumes, which do not allow one to draw any solid conclusion on their connections to coronal plumes. On IRIS SJ 1330 Å and AIA 1600 Å images, we can see that the network regions of R1 and R2 are much brighter than R3 and R4. In particular, the average irradiance of R1 and R2 seen in IRIS SJ 1330 Å is about 2 – 4 times of that in R3 and R4 throughout the entire observing time period.

As shown in Figure 1 and the animations, network jets rooted in the studied regions are very dynamic. In AIA 171 Å images, we also observed many disturbances in the coronal plumes. We speculate that a number of network jets were resulting in disturbances in the coronal plumes. Because of the complex background in both transition region and coronal images, in most of the cases we cannot identify a one-to-one relation between transition region activities and the coronal plume disturbances.

The HMI magnetograms show that the regions are dominated by positive polarities (Figure 1(b)). In agreement with Wang, Warren, and Muglach (2016) and Avallone *et al.* (2018), the regions with clear coronal plumes (R1 and R2) have magnetic features more compact than those in R3 and R4. In most of the regions during the observing period, very few negative polarities were seen in the regions. This indicates that magnetic features with opposite polarity to the major one, if present, should have sizes/lifetimes under the resolution or field strengths under the resolving power (*i.e.* $\sim 10\ \mathrm{Mx\,cm^{-2}}$ in the present case, Liu *et al.*, 2012). To investigate this issue, one will need higher resolution data, which might be provided by the *Goode Solar Telescope* (GST, Goode *et al.*, 2010; Cao *et al.*, 2010), the forthcoming *Daniel K. Inouye Solar Telescope* (DKIST) and the planned *Chinese Advanced Solar Observatories – Ground-based* (ASO-G). Occasionally, we can also observe that small negative polarities appear near the dominant positive ones and immediately disappear within around 1 minute (*i.e.* close to the HMI temporal resolution), thus we cannot link such magnetic activities to any particular network jets.

We examine the magnetic topology of the region using full-disk potential field extrapolations provided by the PFSS package (Schrijver and De Rosa, 2003) in *solarsoft*. In Figure 2, we display the potential field extrapolations of the region based on observations taken on the days from December 1 to December 4, which are tracking the region from the east hemisphere to the west hemisphere. It is clear that the region of interest is dominated by open
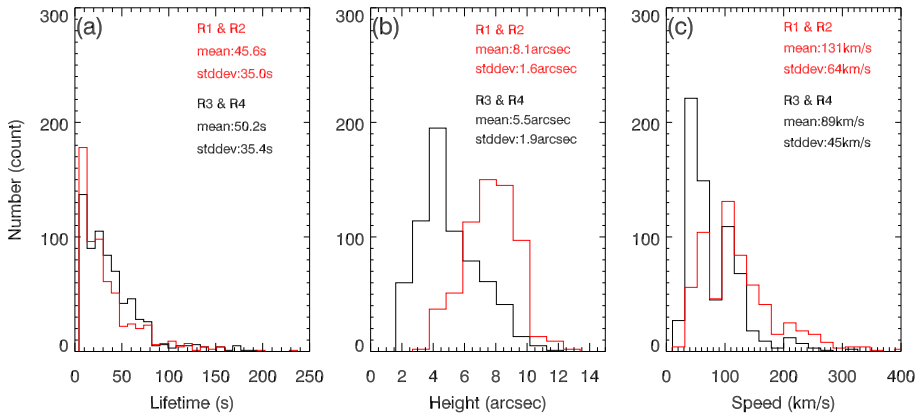
Figure 3 Statistical histograms of the lifetimes (**a**), heights (**b**) and speeds (**c**) of the network jets identified and tracked in the regions of R1 and R2 (*red lines*) and R3 and R4 (*black lines*). The values following "mean" and "stddev" are the mean values and standard deviations of the corresponding parameters, respectively.

field lines which could be seen at least three days before our observations. The open topology of the magnetic field is in agreement with coronal holes observed in the AIA coronal passbands, and it provides a condition for the birth of coronal plumes and network jets. As described above, however, some network lanes in this open field region are rich in coronal plumes but some others are not, while both are rich in network jets. In the following, we will compare the dynamics of the network jets in R1–R4, and investigate the possible relation between coronal plumes and network jets.

4. Statistical Analysis of the Network Jets

In R1–R4, we identify 1293 network jets, of which 619 are located in regions R1 and R2 and the rest 674 located in regions R3 and R4. Based on their coronal plume activities, in the statistics we group network jets from R1 and R2 as one category, and R3 and R4 as another category. The birthrates of network jets in these two types of regions are $7.8 \times 10^{-16} \, \mathrm{m}^{-2} \, \mathrm{s}^{-1}$ (R1 and R2) and $4.7 \times 10^{-16} \, \mathrm{m}^{-2} \, \mathrm{s}^{-1}$ (R3 and R4), respectively. Please note that these birthrates are the lower limits, because we only take into account the network jets that allow for speed calculations (see the Appendix for details). In Figure 3, we give the statistical analysis of three parameters (lifetime, height and speed) of the network jets in the two categories of regions.

In the regions rich in coronal plumes (*i.e.* R1 and R2), the average lifetimes, heights and speeds of all 619 network jets are 45.6 s with a standard deviation (1σ) of 35.0 s, 8.1″ with 1σ of 1.6″ and 131 km s^{-1} with 1σ of 64 km s^{-1}, respectively. In the regions poor in coronal plumes (*i.e.* R3 and R4), the average lifetimes, heights and speeds of all 674 network jets are 50.2 s with 1σ of 35.4 s, 5.5″ with 1σ of 1.9″ and 89 km s^{-1} with 1σ of 45 km s^{-1}, respectively. On average, the network jets from regions rich in coronal plumes are higher and faster than that from the regions poor in coronal plumes. However, we also see that the distributions of each parameter from the two kinds of regions largely overlap. The obtained values of heights and speeds are spreading in the ranges consistent with the measurements in the previous studies (Tian *et al.*, 2014; Narang *et al.*, 2016; Kayshap *et al.*, 2018), but the

mean and most probable values measured here are smaller. This could result from the line-of-sight effect since the region studied here is closer to the disk center than theirs. Although the obtained lifetimes are generally in agreement with the previous studies (Tian *et al.*, 2014; Narang *et al.*, 2016; Kayshap *et al.*, 2018), there is a large portion showing a lifetime of 18 s (*i.e.* two frames in the time series). This kind of short-lifetime jets were not included in the studies of Tian *et al.* (2014) and Narang *et al.* (2016) due to the temporal resolutions of their data, but they appear to be common (see *e.g.* De Pontieu, Martínez-Sykora, and Chintzoglou, 2017; Martínez-Sykora *et al.*, 2017).

In the speed regime, the histograms show two peaks at ~ 50 km s^{-1} and ~ 110 km s^{-1} with a clear division at ~ 90 km s^{-1}. Although with less samples, such a speed distribution has also been observed in Tian *et al.* (2014), but with different peak speeds at ~ 110 km s^{-1} and ~ 160 km s^{-1} and a division at ~ 140 km s^{-1}. Such a difference between their results and ours can be understood if we take into account the line-of-sight effect. The questions are whether such a two-peak distribution is always present and whether this two-peak distribution indicates different species of network jets. These could be interesting topics for future studies using higher cadence data and a larger sample.

The distribution histograms of the lifetimes, heights and speeds of the network jets overlap with those of spicules that also originated from network regions (see *e.g.* Sterling, 2000; Xia *et al.*, 2005; De Pontieu *et al.*, 2007a; Zhang *et al.*, 2012; Pereira, Pontieu, and Carlsson, 2012; Pereira *et al.*, 2014). We speculate that a part of the network jets identified here correspond to spicules in the IRIS SJ 1330 Å passband. Comparing with the speed histogram of spicules (De Pontieu *et al.*, 2007a; Pereira, Pontieu, and Carlsson, 2012), we found that the ratio of the number of the network jets with speeds higher than 100 km s^{-1} to those higher than 50 km s^{-1} is more than 50%, which is much larger than that found in type II spicules.

5. Discussion

Since both network jets and coronal network plumes originate in network regions, the connection between them should be investigated. In the present study, we made a statistical analysis of a few parameters of network jets in four network regions (R1–R4), in which coronal plumes are clearly seen in R1 and R2 but almost invisible in R3 and R4. We found that the network jets in R1 and R2 are statistically higher and faster than those in R3 and R4. These observational results indicate more dynamic and energetic nature of network jets in the regions where coronal plumes are clearly seen. It suggests that the network regions of R1 and R2 could provide a condition in favor of both more energetic network jets and stronger coronal plumes. The coronal plumes belong to the possible sources of the fast solar wind (see Introduction for details). In the present work, we found that the network jets associated with coronal plumes are more energetic and dynamic. The more energetic jets might reach and feed plasma to the corona that could contribute to the mass loss by the solar wind in coronal plumes.

While the unipolar features in R1 and R2 are more compact (implying a higher degree of convergence), it provides stronger compression in the regions. The compression in the footpoints of the magnetic flux tubes might produce shocks that could feed mass and energy to the higher solar atmosphere. The shocks have to be strong and dense enough to power plasma to produce coronal plumes in the region. In this scenario, one would expect that the network jets are also powered by shocks and therefore many network jets should directly feed mass and energy to coronal plumes. This will require a further study using data targeting regions with simpler background (*e.g.* polar regions), which allows one to

identify a one-to-one relation between network jets and coronal plumes. The higher degree of compression might also produce more complicated shearing motions in the footpoints of magnetic flux tubes rooted in the region. The complex shearing motions could generate a complexity of magnetic topology above the photosphere. Such a complexity of the magnetic topology includes magnetic braids (Parker, 1983b,a). As a result of magnetic braiding, magnetic reconnections occur and could heat the plasma to coronal temperatures and accelerate the plasma to more than $100 \, \mathrm{km \, s^{-1}}$ (Cirtain *et al.*, 2013; Huang *et al.*, 2018).

If there were mixed polarities in the region, the higher degree of convergence might directly drive more magnetic reconnection to occur and thus feed more mass and energy to the higher solar atmosphere (He *et al.*, 2010). In the present cases, although there are opposite polarities found near the dominant polarity, they are too rare to agree with the occurrence of the network jets. However, it is possible that many opposite polarities cannot be resolved with the current data, and higher resolution data provided by GST and DKIST might shed light on this problem.

In coronal plumes, propagating disturbances are usually seen (see *e.g.* DeForest and Gurman, 1998; Marsh *et al.*, 2003; De Pontieu *et al.*, 2007b; Wang *et al.*, 2009; De Pontieu and McIntosh, 2010; Tian *et al.*, 2011b,a, 2012, *etc.*). It has been reported that spicules (De Pontieu *et al.*, 2011; Pant *et al.*, 2015; Jiao *et al.*, 2015; Samanta, Pant, and Banerjee, 2015; Jiao *et al.*, 2016) and/or shocks (Hou *et al.*, 2018) could be the possible sources of the propagating disturbances in the coronal plumes. In the present study, the observations show many propagating disturbances along the coronal plumes. We can only speculate from the animation that some of the network jets should be directly linked to the propagating disturbances in the coronal plumes. However, because of the complex background emission, we were not able to identify a one-to-one correspondence between such disturbances and network jets. Whether network jets can directly trigger propagating disturbances in the coronal plumes remains an open question.

The results shown in the present work should be re-examined by more observations, especially those taken during solar minimum. Such data should have a very high cadence, allowing the dynamic network jets to be traced, and the targets should be in or around coronal holes. Furthermore, it is ideal to have two kinds of regions (with and without connection to coronal plumes) in one dataset to avoid uncertainty brought about by line-of-sight and instrumental effects. Unfortunately, searching through the IRIS database, we can say that the dataset analyzed in the present work remains the unique one that is suitable for the purpose. Since many network jets could be spicules that can be observed by ground-based instruments, *e.g.* the *New Vacuum Solar Telescope* (NVST, Liu *et al.*, 2014), the *Swedish Solar Telescope* (SST, Scharmer *et al.*, 2003), GST and DKIST, further studies using high spatial–temporal resolution observations of the chromosphere should shed more light on this topic.

6. Conclusions

In the present study, we studied activities in four regions of network lanes, in which coronal plumes (observed by AIA in the 171 Å passband) are clearly seen being rooted in two (R1 and R2) of the regions but are very faint in the other two (R3 and R4). In all these regions, network jets seen in IRIS SJ 1330 Å passband are abundant. Positive polarities are dominant in these regions and negative polarities could only be seen occasionally. The positive polarities are more compact in R1 and R2, suggesting a higher degree of convergence. The average irradiance of R1 and R2 seen in IRIS SJ 1330 Å is $2-4$ times of that in R3 and R4.

We developed an automatic method to identify and trace network jets in these regions. With the method, we identified and traced 619 network jets in R1 and R2 and 674 in R3 and R4. With these samples, we carried out statistical analyses of lifetimes, heights and speeds of the network jets in R1 and R2 and R3 and R4, respectively. The lifetimes, heights and speeds of the network jets in R1 and R2 are 45.6 s with a standard deviation (1σ) of 35.0 s, 8.1″ with 1σ of 1.6″ and 131 km s^{-1} with 1σ of 64 km s^{-1}, respectively. In R3 and R4, the average lifetimes, heights and speeds of the network jets are 50.2 s with 1σ of 35.4 s, 5.5″ with 1σ of 1.9″ and 89 km s^{-1} with 1σ of 45 km s^{-1}, respectively. These results show that the network jets are on average higher and faster (*i.e.* more dynamic) in the regions with visible coronal plumes than that without clear coronal plumes. The more energetic network jets that are associated with coronal plumes might reach and feed plasma to the corona and then contribute to the balance of the mass loss by the solar wind. We suggest that the convergence of motions at the base of the network regions could build up energy and the energy could be released to the higher solar atmosphere through shocks and/or small-scale (under the current resolution) magnetic reconnections.

Disclosure of Potential Conflicts of Interest   The authors declare that they have no conflicts of interest.

Publisher's Note   Springer Nature remains neutral with regard to jurisdictional claims in published maps and institutional affiliations.

Appendix: Network Jet Identification and Tracking Algorithm

The network jets are identified and traced on the IRIS SJ 1330 Å images by the automatic method. The algorithm of the method includes a few steps as described in the following:

i) Region selection and base definition: In order to simplify the tracking procedures, we analyze the regions R1–R4, where the bright elements in the network lanes (viewed in IRIS SJ 1330 Å) are almost aligned and the network jets are ejected in directions almost parallel to each other. The bases of the network jets in each region are determined as being along the edge of the bright network lanes. Because the network lanes are very dynamic with many transient bright dots, we make an artificial image that is a sum of all the IRIS SJ 1330 Å images taken in the observing period of time, and the edge of the bright network lanes are defined based on the artificial image.

ii) Jet-like feature identification in an image frame: In each region, starting from the bases of the network jets, we select four slices that extend (almost) perpendicular to the network jets and have 1″ separation between each two neighbors (see Figure 4(a)). The variation of the SJ 1330 Å radiance along each slice is then obtained. The local peaks as defined in Huang *et al.* (2017) are identified on the variation curves (see Figure 4(b)). Such a local peak indicates a local brightening. In order to avoid the noise effect, the local peaks with radiances less than 2.5 times of the background are excluded. If a local peak of a slice and the other local peak of the neighboring slice appear at the slice
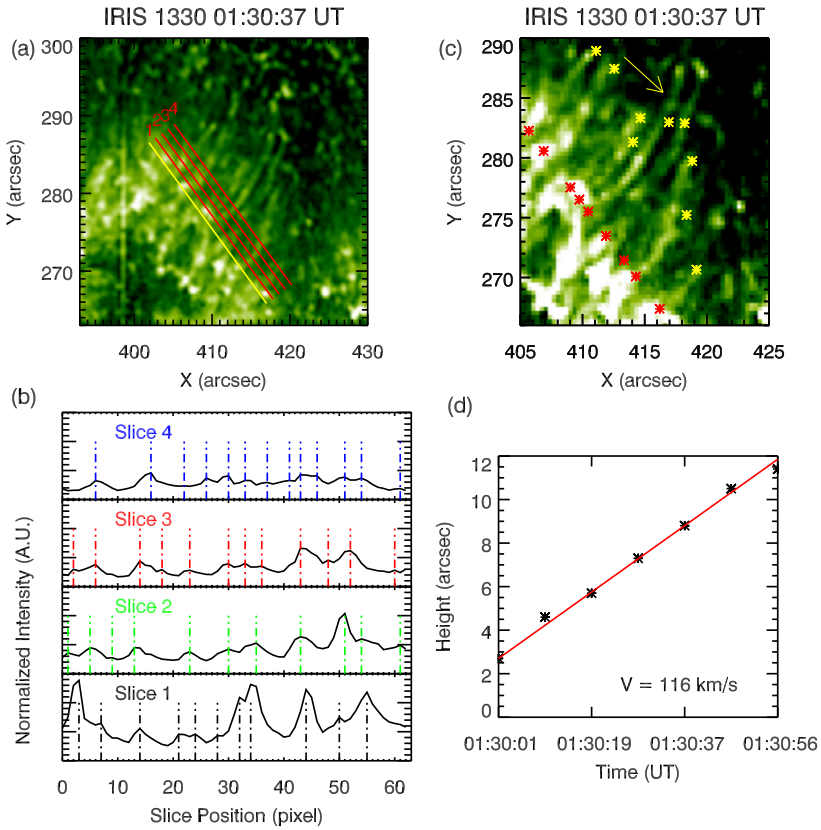
Figure 4 The procedures of the automatic network jet identification and tracking algorithm. (**a**) A network region (R1) observed in IRIS SJ 1330 Å. The *yellow line* indicates the base of the network jets originated in this network. The slices (*red lines* denoted by 1–4) are used to identify jet-like features (see the text for details). (**b**) The IRIS SJ 1330 Å radiation variations along the slices 1–4. The local peaks identified in these variations are denoted by *dash-dotted lines*. (**c**) Examples of identified jet-like features in an image frame at 01:30:37 UT. The *red asterisks* mark the bases of the features and the *yellow asterisks* mark the top of them. The *arrow* points to a network jet that is shown as example in panel (**d**). (**d**) The heights of the network jet (denoted in panel **c**) varying with time. The speed of the network jet is obtained by the slope of the linear fit of this variation (*red line*).

positions with a difference of less than 1″, they are considered to result from the same bright feature. If a bright feature as defined by local peaks is found in all the four slices, it is considered to be a jet-like feature, and its location and propagation direction are determined using the positions of the corresponding local peaks identified in the four slices.

iii) Length determination for the jet-like features: For each identified jet-like feature, a slice along its propagation direction is made and the radiance variation along the slice is obtained. Along the slice, the farthest extending point of the jet-like feature is defined to be the location where the radiance drops below 2.5 times of the background (see Figure 4(c)).

iv) Jet-like feature tracking and definition of network jet and its lifetime and speed: Steps ii) and iii) are run for each image frame. If a jet-like feature found in one frame and the other jet-like feature found in the other close-in-time frame are located at the same

position, they are considered to be the same jet-like feature that is evolving in time. If a jet-like feature is found in more than one image frame and less than 27 image frames (*i.e.* lifetime less than 4 minutes), it is considered to be a network jet. The heights of the network jet seen at different times are given by the lengths of the jet-like features. By following the heights of a network jet at different times, its speed could be obtained using a linear fit in the height *vs.* time plane (see Figure 4(d)). Please note that for each jet only its maximum height is used in the statistics (*i.e.* Figure 3(b)).

References

Avallone, E.A., Tiwari, S.K., Panesar, N.K., Moore, R.L., Winebarger, A.: 2018, Critical magnetic field strengths for solar coronal plumes in quiet regions and coronal holes? *Astrophys. J.* **861**, 111. DOI. ADS.

Cao, W., Gorceix, N., Coulter, R., Ahn, K., Rimmele, T.R., Goode, P.R.: 2010, Scientific instrumentation for the 1.6 m New Solar Telescope in Big Bear. *Astron. Nachr.* **331**, 636. DOI. ADS.

Cirtain, J.W., Golub, L., Winebarger, A.R., De Pontieu, B., Kobayashi, K., Moore, R.L., Walsh, R.W., Korreck, K.E., Weber, M., McCauley, P., Title, A., Kuzin, S., Deforest, C.E.: 2013, Energy release in the solar corona from spatially resolved magnetic braids. *Nature* **493**, 501. DOI. ADS.

Cranmer, S.R.: 2009, Coronal holes. *Living Rev. Solar Phys.* **6**, 3. DOI. ADS.

De Pontieu, B., Martínez-Sykora, J., Chintzoglou, G.: 2017, What causes the high apparent speeds in chromospheric and transition region spicules on the Sun? *Astrophys. J. Lett.* **849**, L7. DOI. ADS.

De Pontieu, B., McIntosh, S.W.: 2010, Quasi-periodic propagating signals in the solar corona: The signature of magnetoacoustic waves or high-velocity upflows? *Astrophys. J.* **722**, 1013. DOI. ADS.

De Pontieu, B., McIntosh, S., Hansteen, V.H., Carlsson, M., Schrijver, C.J., Tarbell, T.D., Title, A.M., Shine, R.A., Suematsu, Y., Tsuneta, S., Katsukawa, Y., Ichimoto, K., Shimizu, T., Nagata, S.: 2007a, A tale of two spicules: The impact of spicules on the magnetic chromosphere. *Publ. Astron. Soc. Japan* **59**, S655. DOI. ADS.

De Pontieu, B., McIntosh, S.W., Carlsson, M., Hansteen, V.H., Tarbell, T.D., Schrijver, C.J., Title, A.M., Shine, R.A., Tsuneta, S., Katsukawa, Y., Ichimoto, K., Suematsu, Y., Shimizu, T., Nagata, S.: 2007b, Chromospheric Alfvénic waves strong enough to power the solar wind. *Science* **318**, 1574. DOI. ADS.

De Pontieu, B., McIntosh, S.W., Carlsson, M., Hansteen, V.H., Tarbell, T.D., Boerner, P., Martinez-Sykora, J., Schrijver, C.J., Title, A.M.: 2011, The origins of hot plasma in the solar corona. *Science* **331**, 55. DOI. ADS.

De Pontieu, B., Title, A.M., Lemen, J.R., Kushner, G.D., Akin, D.J., Allard, B., Berger, T., Boerner, P., Cheung, M., Chou, C., Drake, J.F., Duncan, D.W., Freeland, S., Heyman, G.F., Hoffman, C., Hurlburt, N.E., Lindgren, R.W., Mathur, D., Rehse, R., Sabolish, D., Seguin, R., Schrijver, C.J., Tarbell, T.D., Wülser, J.-P., Wolfson, C.J., Yanari, C., Mudge, J., Nguyen-Phuc, N., Timmons, R., van Bezooijen, R., Weingrod, I., Brookner, R., Butcher, G., Dougherty, B., Eder, J., Knagenhjelm, V., Larsen, S., Mansir, D., Phan, L., Boyle, P., Cheimets, P.N., DeLuca, E.E., Golub, L., Gates, R., Hertz, E., McKillop, S., Park, S., Perry, T., Podgorski, W.A., Reeves, K., Saar, S., Testa, P., Tian, H., Weber, M., Dunn, C., Eccles, S., Jaeggli, S.A., Kankelborg, C.C., Mashburn, K., Pust, N., Springer, L., Carvalho, R., Kleint, L., Marmie, J., Mazmanian, E., Pereira, T.M.D., Sawyer, S., Strong, J., Worden, S.P., Carlsson, M., Hansteen, V.H., Leenaarts, J., Wiesmann, M., Aloise, J., Chu, K.-C., Bush, R.I., Scherrer, P.H., Brekke, P., Martinez-Sykora, J., Lites, B.W., McIntosh, S.W., Uitenbroek, H., Okamoto, T.J., Gummin, M.A., Auker, G., Jerram, P., Pool, P., Waltham, N.: 2014, The Interface Region Imaging Spectrograph (IRIS). *Solar Phys.* **289**, 2733. DOI. ADS.

DeForest, C.E., Gurman, J.B.: 1998, Observation of quasi-periodic compressive waves in solar polar plumes. *Astrophys. J. Lett.* **501**, L217. DOI. ADS.

DeForest, C.E., Lamy, P.L., Llebaria, A.: 2001, Solar polar plume lifetime and coronal hole expansion: Determination from long-term observations. *Astrophys. J.* **560**, 490. DOI. ADS.

DeForest, C.E., Plunkett, S.P., Andrews, M.D.: 2001, Observation of polar plumes at high solar altitudes. *Astrophys. J.* **546**, 569. DOI. ADS.

Deforest, C.E., Hoeksema, J.T., Gurman, J.B., Thompson, B.J., Plunkett, S.P., Howard, R., Harrison, R.C., Hassler, D.M.: 1997, Polar plume anatomy: Results of a coordinated observation. *Solar Phys.* **175**, 393. DOI. ADS.

DeForest, C.E., Howard, R.A., Velli, M., Viall, N., Vourlidas, A.: 2018, The highly structured outer solar corona. *Astrophys. J.* **862**, 18. DOI. ADS.

Del Zanna, G., Bromage, B.J.I.: 1999, The Elephant's Trunk: Spectroscopic diagnostics applied to SOHO/CDS observations of the August 1996 equatorial coronal hole. *J. Geophys. Res.* **104**, 9753. DOI. ADS.

Del Zanna, G., Bromage, B.J.I., Mason, H.E.: 2003, Spectroscopic characteristics of polar plumes. *Astron. Astrophys.* **398**, 743. DOI. ADS.

Doschek, G.A., Landi, E., Warren, H.P., Harra, L.K.: 2010, Bright points and jets in polar coronal holes observed by the Extreme-Ultraviolet Imaging Spectrometer on Hinode. *Astrophys. J.* **710**, 1806. DOI. ADS.

Feng, L., Inhester, B., Solanki, S.K., Wilhelm, K., Wiegelmann, T., Podlipnik, B., Howard, R.A., Plunkett, S.P., Wueser, J.P., Gan, W.Q.: 2009, Stereoscopic polar plume reconstructions from STEREO/SECCHI images. *Astrophys. J.* **700**, 292. DOI. ADS.

Fu, H., Xia, L., Li, B., Huang, Z., Jiao, F., Mou, C.: 2014, Measurements of outflow velocities in on-disk plumes from EIS/Hinode observations. *Astrophys. J.* **794**, 109. DOI. ADS.

Fu, H., Li, B., Li, X., Huang, Z., Mou, C., Jiao, F., Xia, L.: 2015, Coronal sources and in situ properties of the solar winds sampled by ACE during 1999 – 2008. *Solar Phys.* **290**, 1399. DOI. ADS.

Gabriel, A.H., Bely-Dubau, F., Lemaire, P.: 2003, The contribution of polar plumes to the fast solar wind. *Astrophys. J.* **589**, 623. DOI. ADS.

Gabriel, A.H., Abbo, L., Bely-Dubau, F., Llebaria, A., Antonucci, E.: 2005, Solar wind outflow in polar plumes from 1.05 to 2.4 R$_{solar}$. *Astrophys. J. Lett.* **635**, L185. DOI. ADS.

Gabriel, A., Bely-Dubau, F., Tison, E., Wilhelm, K.: 2009, The structure and origin of solar plumes: Network plumes. *Astrophys. J.* **700**, 551. DOI. ADS.

Giordano, S., Antonucci, E., Noci, G., Romoli, M., Kohl, J.L.: 2000, Identification of the coronal sources of the fast solar wind. *Astrophys. J. Lett.* **531**, L79. DOI. ADS.

Goode, P.R., Coulter, R., Gorceix, N., Yurchyshyn, V., Cao, W.: 2010, The NST: First results and some lessons for ATST and EST. *Astron. Nachr.* **331**, 620. DOI. ADS.

Habbal, S.R., Esser, R., Guhathakurta, M., Fisher, R.R.: 1995, Flow properties of the solar wind derived from a two-fluid model with constraints from white light and in situ interplanetary observations. *Geophys. Res. Lett.* **22**, 1465. DOI. ADS.

Hassler, D.M., Dammasch, I.E., Lemaire, P., Brekke, P., Curdt, W., Mason, H.E., Vial, J.-C., Wilhelm, K.: 1999, Solar wind outflow and the chromospheric magnetic network. *Science* **283**, 810. DOI. ADS.

He, J.-S., Marsch, E., Tu, C.-Y., Tian, H., Guo, L.-J.: 2010, Reconfiguration of the coronal magnetic field by means of reconnection driven by photospheric magnetic flux convergence. *Astron. Astrophys.* **510**, A40. DOI. ADS.

Hou, Z., Huang, Z., Xia, L., Li, B., Fu, H.: 2018, Observations of upward propagating waves in the transition region and corona above sunspots. *Astrophys. J.* **855**, 65. DOI. ADS.

Huang, Z., Madjarska, M.S., Doyle, J.G., Lamb, D.A.: 2012, Coronal hole boundaries at small scales. IV. SOT view. Magnetic field properties of small-scale transient brightenings in coronal holes. *Astron. Astrophys.* **548**, A62. DOI. ADS.

Huang, Z., Madjarska, M.S., Scullion, E.M., Xia, L.-D., Doyle, J.G., Ray, T.: 2017, Explosive events in active region observed by IRIS and SST/CRISP. *Mon. Not. Roy. Astron. Soc.* **464**, 1753. DOI. ADS.

Huang, Z., Xia, L., Nelson, C.J., Liu, J., Wiegelmann, T., Tian, H., Klimchuk, J.A., Chen, Y., Li, B.: 2018, Magnetic braids in eruptions of a spiral structure in the solar atmosphere. *Astrophys. J.* **854**, 80. DOI. ADS.

Jiao, F., Xia, L., Li, B., Huang, Z., Li, X., Chandrashekhar, K., Mou, C., Fu, H.: 2015, Sources of quasi-periodic propagating disturbances above a solar polar coronal hole. *Astrophys. J. Lett.* **809**, L17. DOI. ADS.

Jiao, F.-R., Xia, L.-D., Huang, Z.-H., Li, B., Fu, H., Yuan, D., Chandrashekhar, K.: 2016, Damping and power spectra of quasi-periodic intensity disturbances above a solar polar coronal hole. *Res. Astron. Astrophys.* **16**, 93. DOI. ADS.

Kayshap, P., Murawski, K., Srivastava, A.K., Dwivedi, B.N.: 2018, Rotating network jets in the quiet Sun as observed by IRIS. *Astron. Astrophys.* **616**, A99. DOI. ADS.

Lamy, P., Liebaria, A., Koutchmy, S., Reynet, P., Molodensky, M., Howard, R., Schwenn, R., Simnett, G.: 1997, Characterisation of polar plumes from LASCO-C2 images in early 1996. In: Wilson, A. (ed.) *Fifth SOHO Workshop: The Corona and Solar Wind Near Minimum Activity*, *ESA Special Publication* **404**, 487. ADS.

Lemen, J.R., Title, A.M., Akin, D.J., Boerner, P.F., Chou, C., Drake, J.F., Duncan, D.W., Edwards, C.G., Friedlaender, F.M., Heyman, G.F., Hurlburt, N.E., Katz, N.L., Kushner, G.D., Levay, M., Lindgren, R.W., Mathur, D.P., McFeaters, E.L., Mitchell, S., Rehse, R.A., Schrijver, C.J., Springer, L.A., Stern, R.A., Tarbell, T.D., Wueser, J.-P., Wolfson, C.J., Yanari, C., Bookbinder, J.A., Cheimets, P.N., Caldwell, D., Deluca, E.E., Gates, R., Golub, L., Park, S., Podgorski, W.A., Bush, R.I., Scherrer, P.H., Gummin, M.A., Smith, P., Auker, G., Jerram, P., Pool, P., Soufli, R., Windt, D.L., Beardsley, S., Clapp, M., Lang,

J., Waltham, N.: 2012, The Atmospheric Imaging Assembly (AIA) on the Solar Dynamics Observatory (SDO). *Solar Phys.* **275**, 17. DOI. ADS.

Lites, B.W., Card, G., Elmore, D.F., Holzer, T., Lecinski, A., Streander, K.V., Tomczyk, S., Gurman, J.B.: 1999, Dynamics of polar plumes observed at the 1998 February 26 eclipse. *Solar Phys.* **190**, 185. DOI. ADS.

Liu, Y., Hoeksema, J.T., Scherrer, P.H., Schou, J., Couvidat, S., Bush, R.I., Duvall, T.L., Hayashi, K., Sun, X., Zhao, X.: 2012, Comparison of line-of-sight magnetograms taken by the Solar Dynamics Observatory/Helioseismic and Magnetic Imager and Solar and Heliospheric Observatory/Michelson Doppler Imager. *Solar Phys.* **279**, 295. DOI. ADS.

Liu, Z., Xu, J., Gu, B.-Z., Wang, S., You, J.-Q., Shen, L.-X., Lu, R.-W., Jin, Z.-Y., Chen, L.-F., Lou, K., Li, Z., Liu, G.-Q., Xu, Z., Rao, C.-H., Hu, Q.-Q., Li, R.-F., Fu, H.-W., Wang, F., Bao, M.-X., Wu, M.-C., Zhang, B.-R.: 2014, New vacuum solar telescope and observations with high resolution. *Res. Astron. Astrophys.* **14**, 705. DOI. ADS.

Liu, J., McIntosh, S.W., De Moortel, I., Wang, Y.: 2015, On the parallel and perpendicular propagating motions visible in Polar plumes: An incubator for (fast) solar wind acceleration? *Astrophys. J.* **806**, 273. DOI. ADS.

Madjarska, M.S., Huang, Z., Doyle, J.G., Subramanian, S.: 2012, Coronal hole boundaries evolution at small scales. III. EIS and SUMER views. *Astron. Astrophys.* **545**, A67. DOI. ADS.

Marsh, M.S., Walsh, R.W., De Moortel, I., Ireland, J.: 2003, Joint observations of propagating oscillations with SOHO/CDS and TRACE. *Astron. Astrophys.* **404**, L37. DOI. ADS.

Martínez-Sykora, J., De Pontieu, B., Hansteen, V.H., Rouppe van der Voort, L., Carlsson, M., Pereira, T.M.D.: 2017, On the generation of solar spicules and Alfvénic waves. *Science* **356**, 1269. DOI. ADS.

Narang, N., Arbacher, R.T., Tian, H., Banerjee, D., Cranmer, S.R., DeLuca, E.E., McKillop, S.: 2016, Statistical study of network jets observed in the solar transition region: A comparison between coronal holes and quiet-Sun regions. *Solar Phys.* **291**, 1129. DOI. ADS.

Newkirk, G. Jr., Harvey, J.: 1968, Coronal polar plumes. *Solar Phys.* **3**, 321. DOI. ADS.

Panesar, N.K., Sterling, A.C., Moore, R.L.: 2018, Magnetic flux cancelation as the trigger of solar coronal jets in coronal holes. *Astrophys. J.* **853**(2), 189. DOI.

Panesar, N.K., Sterling, A.C., Moore, R.L., Chakrapani, P.: 2016, Magnetic flux cancelation as the trigger of solar quiet-region coronal jets. *Astrophys. J. Lett.* **832**, L7. DOI. ADS.

Panesar, N.K., Sterling, A.C., Moore, R.L., Tiwari, S.K., De Pontieu, B., Norton, A.A.: 2018, IRIS and SDO observations of solar jetlets resulting from network-edge flux cancelation. *Astrophys. J. Lett.* **868**, L27. DOI. ADS.

Pant, V., Dolla, L., Mazumder, R., Banerjee, D., Krishna Prasad, S., Panditi, V.: 2015, Dynamics of on-disk plumes as observed with the Interface Region Imaging Spectrograph, the Atmospheric Imaging Assembly, and the Helioseismic and Magnetic Imager. *Astrophys. J.* **807**, 71. DOI. ADS.

Parker, E.N.: 1983a, Magnetic neutral sheets in evolving fields – Part two – Formation of the solar corona. *Astrophys. J.* **264**, 642. DOI. ADS.

Parker, E.N.: 1983b, Magnetic neutral sheets in evolving fields. I – General theory. *Astrophys. J.* **264**, 635. DOI. ADS.

Patsourakos, S., Vial, J.-C.: 2000, Outflow velocity of interplume regions at the base of polar coronal holes. *Astron. Astrophys.* **359**, L1. ADS.

Pereira, T.M.D., Pontieu, B.D., Carlsson, M.: 2012, Quantifying spicules. *Astrophys. J.* **759**(1), 18. DOI.

Pereira, T.M.D., De Pontieu, B., Carlsson, M., Hansteen, V., Tarbell, T.D., Lemen, J., Title, A., Boerner, P., Hurlburt, N., Wülser, J.P., Martínez-Sykora, J., Kleint, L., Golub, L., McKillop, S., Reeves, K.K., Saar, S., Testa, P., Tian, H., Jaeggli, S., Kankelborg, C.: 2014, An interface region imaging spectrograph first view on solar spicules. *Astrophys. J. Lett.* **792**, L15. DOI. ADS.

Pesnell, W.D., Thompson, B.J., Chamberlin, P.C.: 2012, The Solar Dynamics Observatory (SDO). *Solar Phys.* **275**, 3. DOI. ADS.

Poletto, G.: 2015, Solar coronal plumes. *Living Rev. Solar Phys.* **12**, 7. DOI. ADS.

Pucci, S., Poletto, G., Sterling, A.C., Romoli, M.: 2014, Birth, life, and death of a solar coronal plume. *Astrophys. J.* **793**, 86. DOI. ADS.

Raouafi, N.-E., Stenborg, G.: 2014, Role of transients in the sustainability of solar coronal plumes. *Astrophys. J.* **787**, 118. DOI. ADS.

Raouafi, N.-E., Petrie, G.J.D., Norton, A.A., Henney, C.J., Solanki, S.K.: 2008, Evidence for polar jets as precursors of polar plume formation. *Astrophys. J. Lett.* **682**, L137. DOI. ADS.

Raouafi, N.E., Patsourakos, S., Pariat, E., Young, P.R., Sterling, A.C., Savcheva, A., Shimojo, M., Moreno-Insertis, F., DeVore, C.R., Archontis, V., Török, T., Mason, H., Curdt, W., Meyer, K., Dalmasse, K., Matsui, Y.: 2016, Solar coronal jets: Observations, theory, and modeling. *Space Sci. Rev.* **201**, 1. DOI. ADS.

Rincon, F., Rieutord, M.: 2018, The Sun's supergranulation. *Living Rev. Solar Phys.* **15**(1), 6. DOI.

Samanta, T., Pant, V., Banerjee, D.: 2015, Propagating disturbances in the solar corona and spicular connection. *Astrophys. J. Lett.* **815**, L16. DOI. ADS.

Scharmer, G.B., Bjelksjo, K., Korhonen, T.K., Lindberg, B., Petterson, B.: 2003, The 1-meter Swedish solar telescope. In: Keil, S.L., Avakyan, S.V. (eds.) *Innovative Telescopes and Instrumentation for Solar Astrophysics* **4853**, 341. DOI. ADS.

Schou, J., Scherrer, P.H., Bush, R.I., Wachter, R., Couvidat, S., Rabello-Soares, M.C., Bogart, R.S., Hoeksema, J.T., Liu, Y., Duvall, T.L., Akin, D.J., Allard, B.A., Miles, J.W., Rairden, R., Shine, R.A., Tarbell, T.D., Title, A.M., Wolfson, C.J., Elmore, D.F., Norton, A.A., Tomczyk, S.: 2012, Design and ground calibration of the Helioseismic and Magnetic Imager (HMI) instrument on the Solar Dynamics Observatory (SDO). *Solar Phys.* **275**, 229. DOI. ADS.

Schrijver, C.J., De Rosa, M.L.: 2003, Photospheric and heliospheric magnetic fields. *Solar Phys.* **212**, 165. DOI. ADS.

Sterling, A.C.: 2000, Solar spicules: A review of recent models and targets for future observations – (Invited review). *Solar Phys.* **196**, 79. DOI. ADS.

Sterling, A.C., Moore, R.L., Falconer, D.A., Adams, M.: 2015, Small-scale filament eruptions as the driver of X-ray jets in solar coronal holes. *Nature* **523**, 437. DOI. ADS.

Teriaca, L., Poletto, G., Romoli, M., Biesecker, D.A.: 2003, The nascent solar wind: Origin and acceleration. *Astrophys. J.* **588**, 566. DOI. ADS.

Tian, H., Tu, C., Marsch, E., He, J., Kamio, S.: 2010, The nascent fast solar wind observed by the EUV Imaging Spectrometer on board Hinode. *Astrophys. J. Lett.* **709**, L88. DOI. ADS.

Tian, H., McIntosh, S.W., Habbal, S.R., He, J.: 2011a, Observation of high-speed outflow on plume-like structures of the quiet Sun and coronal holes with Solar Dynamics Observatory/Atmospheric Imaging Assembly. *Astrophys. J.* **736**, 130. DOI. ADS.

Tian, H., McIntosh, S.W., De Pontieu, B., Martínez-Sykora, J., Sechler, M., Wang, X.: 2011b, Two components of the solar coronal emission revealed by extreme-ultraviolet spectroscopic observations. *Astrophys. J.* **738**, 18. DOI. ADS.

Tian, H., McIntosh, S.W., Wang, T., Ofman, L., De Pontieu, B., Innes, D.E., Peter, H.: 2012, Persistent Doppler shift oscillations observed with Hinode/EIS in the solar corona: Spectroscopic signatures of Alfvénic waves and recurring upflows. *Astrophys. J.* **759**, 144. DOI. ADS.

Tian, H., DeLuca, E.E., Cranmer, S.R., De Pontieu, B., Peter, H., Martínez-Sykora, J., Golub, L., McKillop, S., Reeves, K.K., Miralles, M.P., McCauley, P., Saar, S., Testa, P., Weber, M., Murphy, N., Lemen, J., Title, A., Boerner, P., Hurlburt, N., Tarbell, T.D., Wuelser, J.P., Kleint, L., Kankelborg, C., Jaeggli, S., Carlsson, M., Hansteen, V., McIntosh, S.W.: 2014, Prevalence of small-scale jets from the networks of the solar transition region and chromosphere. *Science* **346**(27), 1255711. DOI. ADS.

van de Hulst, H.C.: 1950, On the polar rays of the corona (errata: 11 VIII). *Bull. Astron. Inst. Neth.* **11**, 150. ADS.

Velli, M., Habbal, S.R., Esser, R.: 1994, Coronal plumes and final scale structure in high speed solar wind streams. *Space Sci. Rev.* **70**, 391. DOI. ADS.

Wang, Y.-M.: 1994, Polar plumes and the solar wind. *Astrophys. J. Lett.* **435**, L153. DOI. ADS.

Wang, Y.-M.: 1998, Network activity and the evaporative formation of polar plumes. *Astrophys. J. Lett.* **501**, L145. DOI. ADS.

Wang, Y.-M., Muglach, K.: 2008, Observations of low-latitude coronal plumes. *Solar Phys.* **249**, 17. DOI. ADS.

Wang, Y.-M., Sheeley, N.R. Jr.: 1995, Coronal plumes and their relationship to network activity. *Astrophys. J.* **452**, 457. DOI. ADS.

Wang, Y.-M., Warren, H.P., Muglach, K.: 2016, Converging supergranular flows and the formation of coronal plumes. *Astrophys. J.* **818**, 203. DOI. ADS.

Wang, Y.-M., Sheeley, N.R., Dere, K.P., Duffin, R.T., Howard, R.A., Michels, D.J., Moses, J.D., Harvey, J.W., Branston, D.D., Delaboudinière, J.-P., Artzner, G.E., Hochedez, J.F., Defise, J.M., Catura, R.C., Lemen, J.R., Gurman, J.B., Neupert, W.M., Newmark, J., Thompson, B., Maucherat, A., Clette, F.: 1997, Association of Extreme-Ultraviolet Imaging Telescope (EIT) polar plumes with mixed-polarity magnetic network. *Astrophys. J. Lett.* **484**, L75. DOI. ADS.

Wang, T.J., Ofman, L., Davila, J.M., Mariska, J.T.: 2009, Hinode/EIS observations of propagating low-frequency slow magnetoacoustic waves in fan-like coronal loops. *Astron. Astrophys.* **503**, L25. DOI. ADS.

Wilhelm, K., Dammasch, I.E., Marsch, E., Hassler, D.M.: 2000, On the source regions of the fast solar wind in polar coronal holes. *Astron. Astrophys.* **353**, 749. ADS.

Wilhelm, K., Abbo, L., Auchère, F., Barbey, N., Feng, L., Gabriel, A.H., Giordano, S., Imada, S., Llebaria, A., Matthaeus, W.H., Poletto, G., Raouafi, N.-E., Suess, S.T., Teriaca, L., Wang, Y.-M.: 2011, Morphology, dynamics and plasma parameters of plumes and inter-plume regions in solar coronal holes. *Astron. Astrophys. Rev.* **19**, 35. DOI. ADS.

Withbroe, G.L., Feldman, W.C., Ahluwalia, H.S.: 1991, In: Cox, A.N., Livingston, W.C., Matthews, M.S. (eds.) *The Solar Wind and Its Coronal Origins*, 1087. ADS.

Xia, L.D., Marsch, E., Curdt, W.: 2003, On the outflow in an equatorial coronal hole. *Astron. Astrophys.* **399**, L5. DOI. ADS.

Xia, L.D., Marsch, E., Wilhelm, K.: 2004, On the network structures in solar equatorial coronal holes. Observations of SUMER and MDI on SOHO. *Astron. Astrophys.* **424**, 1025. DOI. ADS.

Xia, L.D., Popescu, M.D., Doyle, J.G., Giannikakis, J.: 2005, Time series study of EUV spicules observed by SUMER/SoHO. *Astron. Astrophys.* **438**, 1115. DOI. ADS.

Yang, S., Zhang, J., Zhang, Z., Zhao, Z., Liu, Y., Song, Q., Yang, S., Bao, X., Li, L., Chu, Z., Li, T.: 2011, Polar plumes observed at the total solar eclipse in 2009. *Sci. China Phys. Mech. Astron.* **54**, 1906. DOI. ADS.

Young, P.R., Klimchuk, J.A., Mason, H.E.: 1999, Temperature and density in a polar plume – Measurements from CDS/SOHO. *Astron. Astrophys.* **350**, 286. ADS.

Zhang, Y.Z., Shibata, K., Wang, J.X., Mao, X.J., Matsumoto, T., Liu, Y., Su, J.T.: 2012, Revision of solar spicule classification. *Astrophys. J.* **750**, 16. DOI. ADS.